HHS Public Access

Author manuscript

J Am Chem Soc. Author manuscript; available in PMC 2023 March 23.

Published in final edited form as:

J Am Chem Soc. 2022 March 23; 144(11): 5087–5098. doi:10.1021/jacs.1c13706.

Mechanism of Radical *S*-Adenosyl-L-methionine Adenosylation: Radical Intermediates and the Catalytic Competence of the 5′-Deoxyadenosyl Radical

Maike N. Lundahl,
Department of Chemistry and Biochemistry, Montana State University, Bozeman, Montana 59717, United States

Raymond Sarksian,
Department of Chemistry and Howard Hughes Medical Institute, University of Illinois at Urbana-Champaign, Urbana, Illinois 61801, United States

Hao Yang,
Department of Chemistry, Northwestern University, Evanston, Illinois 60208, United States

Richard J. Jodts,
Department of Chemistry, Northwestern University, Evanston, Illinois 60208, United States

Adrien Pagnier,
Department of Chemistry and Biochemistry, Montana State University, Bozeman, Montana 59717, United States

Donald F. Smith,
Department of Chemistry and Biochemistry, Montana State University, Bozeman, Montana 59717, United States

Martín A. Mosquera,
Department of Chemistry and Biochemistry, Montana State University, Bozeman, Montana 59717, United States

Wilfred A. van der Donk,
Department of Chemistry and Howard Hughes Medical Institute, University of Illinois at Urbana-Champaign, Urbana, Illinois 61801, United States

[*]**Corresponding Author: Joan B. Broderick** – Department of Chemistry and Biochemistry, Montana State University, Bozeman, Montana 59717, United States; jbroderick@montana.edu.

Author Contributions

The manuscript was written through the contributions of all authors. All authors have given approval to the final version of the manuscript.

Supporting Information

The Supporting Information is available free of charge at https://pubs.acs.org/doi/10.1021/jacs.1c13706.

Synthetic methods, MS data, depictions of structures used in DFT calculations, depictions of energy-minimized structures, EPR spectra and simulations, tables of hyperfine tensors and spin quantitation information, coordinates used in DFT calculations (PDF)

Complete contact information is available at: https://pubs.acs.org/10.1021/jacs.1c13706

The authors declare no competing financial interest.

NOTE ADDED IN PROOF

Following acceptance of this paper, a computation-only paper appeared in the literature, concluding that Ω is not an organometallic species.[77] We do not agree with the method or conclusions of this work and this will be addressed in future reports.

Brian M. Hoffman,
Department of Chemistry, Northwestern University, Evanston, Illinois 60208, United States

William E. Broderick,
Department of Chemistry and Biochemistry, Montana State University, Bozeman, Montana 59717, United States

Joan B. Broderick*
Department of Chemistry and Biochemistry, Montana State University, Bozeman, Montana 59717, United States

Abstract

Radical *S*-adenosyl-L-methionine (SAM) enzymes employ a [4Fe–4S] cluster and SAM to initiate diverse radical reactions via either H-atom abstraction or substrate adenosylation. Here we use freeze-quench techniques together with electron paramagnetic resonance (EPR) spectroscopy to provide snapshots of the reaction pathway in an adenosylation reaction catalyzed by the radical SAM enzyme pyruvate formate-lyase activating enzyme on a peptide substrate containing a dehydroalanine residue in place of the target glycine. The reaction proceeds via the initial formation of the organometallic intermediate Ω, as evidenced by the characteristic EPR signal with $g_{\parallel}$ = 2.035 and $g_{\perp}$ = 2.004 observed when the reaction is freeze-quenched at 500 ms. Thermal annealing of frozen Ω converts it into a second paramagnetic species centered at g_{iso} = 2.004; this second species was generated directly using freeze-quench at intermediate times (~8 s) and unequivocally identified via isotopic labeling and EPR spectroscopy as the tertiary peptide radical resulting from adenosylation of the peptide substrate. An additional paramagnetic species observed in samples quenched at intermediate times was revealed through thermal annealing while frozen and spectral subtraction as the SAM-derived 5′-deoxyadenosyl radical (5′-dAdo•). The time course of the 5′-dAdo• and tertiary peptide radical EPR signals reveals that the former generates the latter. These results thus support a mechanism in which Ω liberates 5′-dAdo• by Fe–C5′ bond homolysis, and the 5′-dAdo• attacks the dehydroalanine residue of the peptide substrate to form the adenosylated peptide radical species. The results thus provide a picture of a catalytically competent 5′-dAdo• intermediate trapped just prior to reaction with the substrate.

Graphical Abstarct

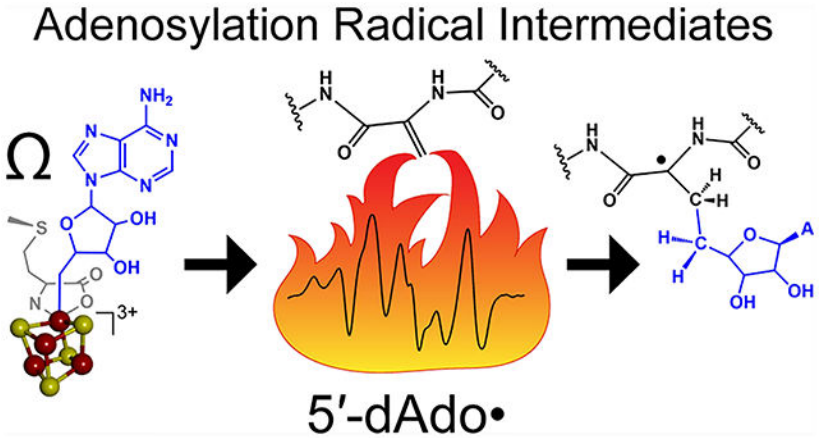

INTRODUCTION

Radical *S*-adenosyl-L-methionine (SAM) enzymes are found in all domains of life and catalyze an astounding array of reactions, some of which have potential applications in the biosynthesis of pharmaceutically or technologically useful compounds, such as antibiotics or biofuels.[1–7] Radical SAM (RS) enzymes have a partial or full TIM barrel fold structure[8] and bind a site-differentiated [4Fe–4S] cluster with three cysteines from a conserved CX_3CX_2C motif.[9] The unique iron of the [4Fe–4S] cluster is coordinated by the amino and carboxylate moieties of SAM to form a coordination complex central to the catalytic mechanism.[10–13] Catalysis by RS enzymes is initiated via electron transfer from the reduced $[4Fe–4S]^{1+}$ cluster to the sulfonium of SAM,[14,15] resulting in reductive cleavage of the S–C5′ bond of SAM;[16–18] this reductive cleavage leads to the formation of an organometallic intermediate Ω in which the 5′-C of the 5′-deoxyadenosyl fragment is directly bound to the unique iron of the [4Fe–4S] cluster.[19,20] While initially surprising, Ω has been observed in a wide range of RS enzymes[20–22] and is proposed to be a key intermediate across the RS superfamily.[20] Synthetic models of Ω developed by Suess and coworkers have provided further insight into this species.[23–25] In the reaction of the RS enzyme pyruvate formate-lyase activating enzyme (PFL-AE) with its substrate pyruvate formate-lyase (PFL), Ω is shown to convert cleanly to the product glycyl radical upon thermal annealing, demonstrating the catalytic competence of Ω.[19] In RS reactions, it is proposed that homolysis of the Ω Fe–C5′ bond yields the 5′-deoxyadenosyl radical (5′-dAdo•) that subsequently abstracts a hydrogen atom from the substrate to initiate catalysis in the majority of characterized RS enzymes (Figure 1a).[26]

In rarer cases, the 5′-dAdo• instead directly adds to an sp^2 carbon of a substrate double bond to yield an adenosylated product (Figure 1b). RS adenosylation plays key roles in important natural product biosynthetic pathways.[6] For example, RS adenosylation catalyzed by aminofutilosine synthase (MqnE) is central to the biosynthetic aminofutilosine pathway to produce menaquinone (vitamin K_2). This pathway is essential for several pathogenic bacteria but not for those in the human gut microbiome,[27–29] making the aminofutilosine pathway a target for antibiotic discovery.[28] In another example, the RS enzyme HpnH catalyzes adenosylation of hopene in the biosynthetic pathway for bacteriohopanepolyol production.[30,31] Undoubtedly additional natural adenosylation reactions will be uncovered as more RS enzyme reactivities are characterized.

Evidence for the 5′-dAdo• intermediate central to RS reactions includes label transfer from substrate to the 5′-dAdoH formed from SAM during turnover,[16,17,32,33] as well as the characterization of an allylically stabilized anhydroadenosyl radical analog;[34–36] 5′-dAdo• itself, however, eluded direct detection for decades. A major breakthrough came with the recognition that the $[4Fe–4S]^+$/SAM complex is photochemically active, allowing reductive cleavage to be induced by cryogenic irradiation with blue light;[37] in the RS enzyme PFL-AE such irradiation cleanly generated the 5′-dAdo• in the absence of substrate, which allowed its full and detailed characterization through electron paramagnetic resonance (EPR) and electron-nuclear double resonance (ENDOR) spectroscopies.[37] Subsequent studies showed that other RS enzymes also undergo photolysis of the active site $[4Fe–4S]^+$/SAM complex, with some generating 5′-dAdo• and others generating an SAM-derived $•CH_3$ radical via

regioselective cleavage of the S–CH_3 bond of SAM.[38,39] These alternative photochemical outcomes led to a new understanding of the basis for regioselective reductive C–S bond cleavage of SAM in RS enzymes.[39] An alternative strategy for the capture of the 5′-dAdo• involved the use of a non-native substrate with HydG; *cis-p*-coumaric acid used in place of tyrosine was found to initiate reductive cleavage of SAM but prevented substrate H-atom abstraction,[40] yielding a mixture of paramagnetic species, one of which was characterized by EPR spectroscopy as the 5′-dAdo•.[40] However, under enzyme catalytic turnover conditions, the 5′-dAdo• radical has yet to be observed, and it has been suggested that the 5′-dAdo• may never be free, and 5′-dAdo• formation may be concerted with H-atom abstraction.[5,36,41]

The 5′-dAdo• has also been ‘captured’ via its propensity for addition to olefinic groups.[42–49] For example, PFL-AE normally catalyzes H-atom abstraction from the G734 residue of PFL to generate the catalytically essential glycyl radical of PFL.[50,51] This reactivity was modeled using an heptamer peptide substrate analog (RVSGYAV),[52] which mimics the G734 loop of PFL and binds such that the G734 *pro-S* hydrogen is positioned 3.9 Å away from the 5′-C of coordinated SAM.[53] However, using a similar peptide (Suc-RVP(Dha)YAVR-NH_2; Suc, succinyl) in which Ser733 is replaced by proline and Gly734 is replaced with dehydroalanine (Dha), Knappe and coworkers observed adenosylation at the olefinic *β*-carbon of Dha rather than H-atom abstraction of the *pro-S* G734 H-atom.[43] Similarly, the RS enzyme QueE normally catalyzes a heterocyclic ring condensation initiated by H-atom abstraction, but when presented with 6-carboxypterin (6-CP) as a substrate analog it instead catalyzes adenosylation at a double bond of 6-CP to yield an adenosylated 6-CP radical species.[45] In the case of B_{12} enzymes, Banerjee and coworkers showed that in methylmalonyl-CoA mutase, a substrate analog presenting a double bond in place of the abstractable H-atom underwent adenosylation, resulting in a stable bi-radical species consisting of the adenosylation-product tertiary carbon radical plus Co(II)-cobalamin.[42] Despite the ability to generate 5′-dAdo• in the absence of a competent substrate, and the evidence for 5′-dAdo• involvement in RS enzymes, key questions remain. Among the most central: is the 5′-dAdo• radical a true intermediate that is observable during RS enzymatic reactions?

Here we examine the mechanistic details of a radical SAM adenosylation reaction catalyzed by PFL-AE on a model octamer peptide substrate (RVS(Dha)YAVR) in which the only change from the wild-type sequence is the replacement of the target Gly734 residue by Dha (Figure 2). We show that PFL-AE catalyzes the adenosylation of this Dha peptide (Dha-pep). Upon freeze-quench trapping, the reaction of reduced PFL-AE with SAM and Dha-pep gives the central RS paramagnetic organometallic intermediate Ω. Upon thermal annealing, Ω converts to a subsequent paramagnetic species with EPR parameters consistent with an adenosylated tertiary peptide radical intermediate, demonstrating that Ω is catalytically competent. The adenosylated peptide radical intermediate (Ado-Dha-pep•) was directly freeze trapped at intermediate reaction times and unequivocally identified and characterized as containing the adenosylation-product tertiary carbon radical by EPR spectroscopy combined with isotopic labeling and density functional theory (DFT) calculations. Closer examination of intermediate reaction time freeze-quench samples revealed a second paramagnetic species that we identify as the elusive 5′-dAdo• radical intermediate. We

further show that this 5′-dAdo• intermediate is catalytically involved, being captured in the act of substrate adenosylation.

EXPERIMENTAL SECTION

Materials.

All reagents were purchased from MilliporeSigma at the highest available purity unless otherwise noted. Fmoc-amino acids with appropriate side-chain protecting groups were purchased from Chem-Impex Intl. and used without further purification. D_2-cysteine was purchased from Cambridge Isotope Laboratories, Inc. Sodium dithionite, D_2O, and sodium sulfide were obtained from Acros Organics. Tris (hydroxymethyl) aminomethane (Tris) was purchased from Research Products International. All spectroscopy samples were prepared under an anaerobic atmosphere in a mBraun glove box (O_2 < 8 ppm) or in a COY chamber (O_2 < 10 ppm).

Synthesis of Peptides.

The syntheses of the Dha-containing peptides, RVS(Dha)YAVR and RVS(D_2-Dha)YAVR, were carried out using modifications of published procedures,[54,55] with D_2-Cys serving as the precursor for D_2-Dha in the latter. Detailed procedures are provided in the SI.

Expression and Purification of PFL-AE.

Expression and purification PFL-AE was carried out following a published protocol with no modification.[20]

Enzymatic SAM Synthesis.

Natural abundant and isotopically labeled SAM were synthesized as previously described.[18,56] The purification of SAM was carried out following a previously published protocol.[56]

NMR Spectroscopy.

^{1}H NMR spectroscopy was recorded at 500 MHz, and ^{13}C NMR was recorded at 126 MHz on a Bruker 500 MHz spectrometer. NMR spectra were referenced to residual chloroform (^{1}H, 7.26 ppm; ^{13}C, 77.2 ppm). Chemical shifts are reported in parts per million (ppm), and multiplicities are indicated for observed splitting. Coupling constants are indicated in Hertz.

MALDI-TOF MS.

MALDI-TOF MS data (Figures S1 and S2) were acquired on a Bruker UltrafleXtreme MALDI-TOF/TOF mass spectrometer. Samples were desalted using C18 ZipTips and co-spotted with Super-DHB as the matrix.

Preparation of LC–MS Samples.

A 45 μL solution of 385 μM RVS(Dha)YAVR peptide, 225 μM PFL-AE, 6.75 mM sodium dithionite, and 2.25 mM SAM in a 50 mM Tris–Cl pH 8.5, 100 mM KCl, 10% glycerol buffer was allowed to react for 10 min. The solution was then quenched with 5 μL of 400

mM acetic acid pH 4.5 and incubated on ice for 30 min prior to centrifugation for 10 min at 13,000 rpm at 4 °C to remove precipitated protein. A control sample was made using the same method excluding SAM.

LC–MS.

All LC–MS experiments were performed at the Montana State University Proteomics, Metabolomics, and Mass Spectrometry Facility. An Agilent 1290 LC was coupled to an Agilent 6538 quadrupole time-of-flight mass spectrometer. Liquid chromatography was performed on a Waters Acquity C_{18} HSST3 column (1.8 um particle size, 2.1 × 100 mm) maintained at 50 °C and operated at a flow rate of 0.4 mL/min. The mobile phase consisted of water (0.1% formic acid) as solvent A and acetonitrile (0.1% formic acid) as solvent B. The initial mobile phase conditions were 95% A and 5% B (held for 1 min). A linear gradient profile was used over 8 min to 95% B, followed by a hold of 1 min at the original conditions for column re-equilibration. The total run time per sample was 12 min.

The LC eluent was coupled to an electrospray ionization source operating in the positive-ion mode. The mass spectrometer was operated at 1 Hz over a mass range of 100–1700 m/z at a scan rate of 1 Hz.

EPR Sample Preparation.

At room temperature, a solution of PFL-AE was reduced with sodium dithionite for 8 min before it was added to a solution of Dha peptide and SAM in an X-band EPR tube (Wilmad LabGlass, 4 mm OD). The resulting mixture of these solutions yielded a sample with the following concentrations: 225 μM PFL-AE, 385 μM Dha peptide, 6.75 mM sodium dithionite, 2.25 mM SAM in buffer (50 mM Tris–Cl, pH 8.5, 100 mM KCl, 10% glycerol). The samples were flash frozen in liquid nitrogen at times indicated.

RFQ Sample Preparation.

Rapid freeze-quench (RFQ) experiments were performed using a protocol previously described in order to protect the protein from oxygen despite the RFQ instrument not being placed in an anaerobic environment.[19,20] A solution of PFL-AE was reduced with sodium dithionite for 8 min before it was loaded into one loop while a Dha peptide, and SAM mixture was loaded into the other loop, achieving a post-mixing ratio of 1:1.7 of PFL-AE:Dha peptide. The mixing of these solutions yielded a sample with the following concentrations: 225 μM PFL-AE, 385 μM Dha peptide, 6.75 mM sodium dithionite, 2.25 mM SAM in buffer (50 mM Tris–Cl pH 8.5, 100 mM KCl, 10% glycerol). The sample loops were connected to a System 100 apparatus from Update Instrument and rapidly mixed. The mixture was quenched by spraying onto two rotating aluminum-coated copper wheels cooled in liquid nitrogen, at mixing times of 500 ms, 1 and 2 s. The frozen powder was collected in a funnel and packed into precision Q-band tubes (2.5 mm OD) for X-band EPR analysis. The variations in packing density precluded precise spin quantitations.

Continuous Wave EPR Spectroscopy.

X-band continuous wave (CW) spectroscopy on hand-quenched samples was conducted at Montana State University using a Bruker EMX EPR spectrometer equipped with a

Bruker/Cold Edge (Sumitomo Cryogenics) 10 K waveguide cryogen-free system with an Oxford MercuryiTC controller unit and helium Stinger recirculating unit (Sumitomo Cryogenics, ColdEdge Technologies). Spectra were recorded at 40–70 K at 9.38 GHz using 3.0 G modulation amplitude and 3 mW power. Quantification of the spin concentration of 5′-dAdo• and Ado-Dha-pep• was achieved by comparison of the double integral of the EPR intensity to that of a standard curve made from solutions of 4.73–94.6 μM TEMPO radical in DI H_2O (see SI; Tables S2–S4). X-band CW EPR spectroscopy performed on the RFQ samples was conducted at Northwestern University using a Bruker ESP 300 spectrometer equipped with an Oxford Instruments ESR 910 continuous helium flow cryostat. Experimental parameters were 40 K, 9.37 GHz, 2 mW microwave power, 100 kHz modulation, and 5 G modulation amplitude. Simulations of experimental spectra were performed using EasySpin 5.2.30[57] within the Matlab R2020b software suite (The Mathworks Inc.).

Models for Dha-pep Binding.

A model of the RVS(Dha)YAVR peptide in the active site of PFL-AE was generated from the crystallographically determined structure of PFL-AE, SAM, and RVSGYAV peptide (PDB: 3CB8)[53] by changing the central Gly residue (Gly734 of PFL) to a Dha residue. This modified structure was optimized using the "molecular sculpting" plugin in PyMOL[58] in order to avoid steric clashes and to provide reasonable molecular geometries. For the model of the adenosylated peptide (Ado-Dha-pep•) in the active site of PFL-AE, the model described above was used with the following modifications. SAM was manually cleaved at the S–C5′ bond, and the Dha residue was changed to an alanine. Then, the dAdo moiety was manually translated to be in close proximity to the alanine to create the C–C bond between C5′ of dAdo and C_β of alanine. This structure was optimized using the "molecular sculpting" plugin in PyMOL[58] (The PyMOL Molecular Graphics System, Version 2.3.4, Schrödinger, LLC).

DFT Calculations.

All DFT computations were carried out with the ORCA 4.2.1 software package.[59–61] A simplified model for the Ado-Dha-pep• was generated by truncating the peptide between the C_α and N of Ser733 and between N and C_α of Tyr735 (Figure S3). The geometry around the Gly734 C_α was changed to a planar sp^2 radical configuration, a CH_2–CH_3 was added to approximate the Dha C_β and the adenosyl moiety, and hydrogen atoms were added to the truncated ends. The initial geometry for this simplified model was taken from the crystallographically determined structure of the RVSGYAV peptide bound to PFL-AE (PDB 3CB8).[53] Input coordinates for the geometry optimizations were generated using Avogadro,[62,63] and both unconstrained and constrained geometry optimizations were calculated. In the constrained geometry, the nonhydrogen atoms in the peptide fragment were fixed to the crystallographically determined geometry, while the Ado-Dha C_β and the 5′-C were allowed to find their lowest energy geometry. The constrained geometry held the dihedral angle between the C_α–N and the C_β–H_b at 20° and yielded a better match to experiment, implying the dihedral angle between the C_α–N and the $2p\pi$ orbital of the C_β–H_b is 70°. Geometry optimization calculations utilized the B3LYP/G hybrid functional[64–66] and the Ahlrichs' valence triple-ξ with a polarization function basis set.[67,68] These input

coordinates were also used in calculations using Becke's functional for exchange along with Perdew's functional for correlation (BP86) for comparison.[64,66] Hyperfine and *g*-tensors were calculated for all the input geometries by the coupled-perturbed self-consistent field approach using the B3LYP and BP86 hybrid functionals and EPR-III basis set[69,70] and in combination with an accurate spin–orbit coupling operator [RI-SOMF(1X)].[71]

RESULTS

Synthesis of a Dehydroalanine Peptide Substrate.

To probe the mechanistic details of RS adenosylation using PFL-AE, a PFL substrate analog presenting a double bond rather than an abstractable hydrogen was needed to enable adenosylation reactivity. An 8-mer peptide corresponding to the sequence surrounding the target Gly734 of PFL was synthesized, with the only modification from the wild-type sequence being the substitution of Dha for Gly734: RVS(Dha)YAVR (Figure 2), referred to hereafter as Dha-pep. Dha-pep differed from the Suc-RVP(Dha)YAVR-NH_2 peptide used by Knappe and coworkers,[43] which included a proline in place of the serine adjacent to Dha because it was necessary to prevent side reactions with the native Ser during the introduction of the Dha;[43] improvements in peptide synthesis methodology since the time of Knappe's report allowed us to synthesize Dha-pep with the exact sequence of the G734 loop in PFL.[54,55]

Adenosylation of Dha-pep by PFL-AE.

Upon reaction of reduced PFL-AE with SAM and Dha-pep, the addition of an adenosyl moiety to Dha-pep was observed by LCMS (Figure S4). This result demonstrates that PFL-AE, when presented with the double bond of Dha-pep rather than an abstractable hydrogen, can catalyze an RS adenosylation as an alternative to its natural H-atom abstraction reaction. The rest of this report describes studies of the mechanism of this reaction.

Reaction of PFL-AE with SAM when Dha-pep Is Bound Yields the Organometallic Intermediate Ω.

Time-dependent RFQ EPR measurements were performed to probe the reaction course of PFL-AE with Dha-pep and SAM. Freeze-quench at 500 ms shows an EPR signal with $g_{\parallel}$ = 2.035 and $g_{\perp}$ = 2.004, associated with the organometallic intermediate Ω, in which C5′ of a SAM-derived adenosyl moiety is covalently bound to the unique iron of the [4Fe–4S] active site cluster (Figure 3A).[19] Ω is a key intermediate in a wide range of RS catalyzed reactions.[20–22,72,73] The formation of Ω is initiated by electron transfer from the $[4Fe–4S]^{1+}$ cluster to SAM. This cleaves the S–C5′ bond, producing 5′-dAdo•, which rapidly forms a covalent bond between C5′ and the unique Fe of $[4Fe–4S]^{3+}$ (Scheme 1). In the reaction with Dha-pep, the EPR intensity of Ω as measured at 40 K grows with quench time until it maximizes at 2 s (Figure 3A).

To examine the fate of Ω in this reaction, a 2 s RFQ sample exhibiting a strong Ω EPR signal was annealed while frozen at progressively higher temperatures, with re-cooling to 40 K for examination by EPR spectroscopy at each stage (Figure 3B). The Ω EPR signal is stable when warmed for 1 min at 180 K; however, it substantially diminishes during a few minutes

of annealing at 220 K and is fully lost upon annealing for a few minutes at 240 K. As the Ω signal disappears, it is replaced by a hyperfine-split radical signal, indicating the progression from Ω to a subsequent radical intermediate in the reaction.

Capture of a Tertiary Carbon Radical Intermediate.

The observation of Ω formation during the adenosylation reaction leads to a proposed mechanism of RS adenosylation that, like RS H-atom abstraction, involves the liberation of 5′-dAdo• by homolysis of the Fe–C5′ bond of Ω. In the present case, this is followed by an attack of the 5′-dAdo• on the terminal sp^2 carbon of the Dha double bond to yield an adenosylated tertiary substrate radical intermediate, Ado-Dha-pep•, with the odd electron located in a 2pπ orbital on C_α of Dha, Scheme 1. The Ado-Dha-pep• is presumably quenched by solvent, with the electron being provided by dithionite. To trap the Ado-Dha-pep• intermediate, the reaction of PFL-AE with SAM and Dha-pep was freeze-quenched ~8 s after mixing and examined by EPR spectroscopy at 70 K. The resulting sample exhibited an EPR signal with a symmetric triplet formed from overlapping doublets, centered at g_{iso} = 2.004 (Figure 4A). A simulation including isotropic ^{1}H hyperfine couplings of 45 and 30 MHz provides an excellent fit to the experimental spectrum.

The same experiment carried out with C_β–[D_2]-Dha-pep shows that the a_{iso}(H) = 45 MHz coupling is lost upon deuteration of the C_β protons, leaving only the smaller 30 MHz splitting (Figure 4B). Thus, we attribute the 45 MHz coupling to one of the two C_β–H atoms of Dha. The reaction of reduced PFL-AE with Dha peptide and [adenosyl-$^{13}C_{10}$,$^{15}N_5$]-SAM results in an EPR spectrum with a large additional splitting (Figure 4C), a_{iso} = 48 MHz, which is assigned as the β-type coupling of ^{13}C5′ to the spin on C_α of the former Dha in the Ado-Dha-pep• intermediate.

Given that reaction of PFL-AE with SAM and C_β–[D_2]-Dha-pep gives a radical intermediate that retains the 30 MHz splitting (Figure 4B), the ^{1}H giving this hyperfine coupling cannot be either of the C_β protons. To determine whether the 30 MHz coupling is due to the adjacent amide N–H, the reaction of reduced PFL-AE with SAM and Dha peptide was carried out in 95% D_2O, leading to loss of the a_{iso}(H) = 30 MHz coupling and leaving a doublet with a_{iso}(H) = 45 MHz (Figure 4D). Peptide backbone amide hydrogen atoms readily undergo H/D exchange when incubated in D_2O, and thus the 30 MHz coupling lost upon reaction in D_2O can be assigned to the amide hydrogen adjacent to the Dha C_α–carbon radical site. This assignment is further supported by the observation of a singlet EPR signal when the reaction with C_β–[D_2]-Dha-pep is carried out in D_2O, leading to a peptide radical with no C_β–H or N–H protons (Figure 4E).

These results show that the two hyperfine couplings observed for the unlabeled Dha-pep in H_2O arise from one of the C_β–H protons and the exchangeable amide N–H proton; the second C_β–H proton must have a hyperfine coupling that is too small to be resolved. Together, these observations establish that the EPR signal observed for the ~8 s freeze-quenched reaction indeed arises from the radical product of catalytic adenosylation, Ado-Dha-pep• (Scheme 1).

Structure of the Tertiary Carbon Radical Intermediate.

The finding that the resolved hyperfine splitting of Ado-Dha-pep• arises from one of the C_β–H protons and the amide N–H proton provides insight into the conformation of the adenosylated Dha peptide radical in these experiments, which we have evaluated by using DFT to compute hyperfine couplings. A simplified model of Ado-Dha-pep• (Figure S3), truncated at the C_α of Ser733 and the amide nitrogen of Tyr735, and using CH_3 to model the adenosyl group on Ado-Dha C_β, was given a fixed peptide backbone conformation based on the structure of the wild-type PFL peptide ($RVSG_{734}YAV$) bound in the PFL-AE active site (PDB: 3CB8), except that the geometry around the C_α of Gly734 was changed to a planar sp^2 radical configuration. This fixed conformation imposes a dihedral angle of ~50° between the C_α radical $2p\pi$ orbital and the adjacent N–H bond (Figure 5). The C_α–C_β bond was rotated to find the orientation providing the best match to the experimentally determined hyperfine couplings (SI), both the observed coupling to one of the C_β–H protons and the absence of a resolved coupling to the other, and led to the dihedral angles shown in Figure 5. Calculations were also carried out for a fully energy-minimized C_α–N–H structure, a planar conformation allowing for greater delocalization and thus stabilization of the $2p\pi$ unpaired electron; however, the resulting hyperfine couplings did not match the experimental results (Table 1 and Figures S5, S6, SI). The DFT calculations in conjunction with the experimental data thus support an adenosylated peptide radical intermediate that is constrained in the active site of PFL-AE with a conformation similar to that observed for the wild-type peptide bound to the PFL-AE active site.

5′-dAdo• as an Adenosylation Intermediate.

During the course of trapping and characterizing the tertiary Ado-Dha-pep• intermediate, we observed a second, quench-time-dependent EPR signal at 40 K overlapping that of the Ado-Dha-pep•, as evidenced by the additional features apparent just outside the strong Ado-Dha-pep• signal (Figure 6A, top). This signal is suppressed at higher temperatures, which explains its absence in the 70 K spectra of Figure 4. To evaluate this additional signal in more detail, a sample freeze-quenched after 10 s (Figure 6A, top) was annealed at 125 K for 15 min; its EPR spectrum was recorded at 40 K (Figure 6A, bottom) revealed significant loss of this additional signal. The annealed spectrum was scaled by a factor of 0.93 (since the Ado-Dha-pep• signal increased upon annealing) and then subtracted from the unannealed sample, revealing the additional signal (Figure 6B) to be nearly identical to the previously reported 5′-dAdo• EPR signal generated by photolysis of reduced PFL-AE with SAM bound.[37] The simulation parameters for the 5′-dAdo• obtained here and from our prior report (Table S1) are identical except for the coupling to C4′, which indicates a slightly different torsion angle around the C4′–C5′ bond.[37]

Analysis of the 40 K EPR spectra before and after annealing shows that the 5′-dAdo• EPR signal decreases from ~30 to 15% of total spin intensity with annealing, while the Ado-Dha-pep• signal increases from ~70 to 85% of total spin intensity (Table S2), consistent with conversion of the 5′-dAdo• to the product Ado-Dha-pep•; this result suggests that the observed 5′-dAdo• is a trapped catalytically competent intermediate.

To test the mechanistic role of this 5′-dAdo•, we evaluated the time progression of the formation of the Ado-Dha-pep• and loss of 5′-dAdo• through a series of experiments with freeze-quench delay times of 8 to 18 s (Figure 7A). The quench-time dependence of the intensities in these spectra (Figure 7B) reveals that 5′-dAdo• EPR signal is lost concomitantly with an increase in the Ado-Dha-pep• signal. Together, the annealing of 5′-dAdo• to Ado-Dha-pep• (Figure 6) and of the time course of the conversion of 5′-dAdo• to Ado-Dha-pep• (Figure 7) establish that the 5′-dAdo• observed in these experiments indeed is a catalytically competent intermediate that is formed by liberation from Ω and caught in the act of adenosylating the Dha peptide.

In both freeze-quench time course and annealing experiments, there is some overall loss of the Ado-Dha-pep• EPR signal with time, which we attribute to solvent quenching of the Ado-Dha-pep•. This explanation is consistent with the observation that Ado-Dha-pep• signals are more intense when experiments are carried out in D_2O (Figure S7), where a solvent kinetic isotope effect would be expected to slow solvent quenching. Solvent quenching is not an important factor in H-atom abstraction from the native substrate PFL,[74] because the Gly734 radical thus formed is on a protein loop of PFL that becomes buried in the interior of the 170 kDa PFL protein subsequent to its activation by PFL-AE.[75,76] In contrast, the C_α tertiary carbon Ado-Dha-pep• on the smaller Dha-pep peptide substrate is solvent exposed when bound to PFL-AE and therefore susceptible to quenching and more difficult to capture, except with short reaction times.

DISCUSSION

RS enzymes catalyze diverse radical reactions through a key organometallic intermediate Ω that is formed upon the reductive cleavage of SAM.[19,20] The long-implicated 5′-dAdo• intermediate has also been observed, but to date its trapping has required either cryogenic photoinduced electron transfer in the RS enzyme/$[4Fe–4S]^+$/SAM complex in the absence of substrate[37,39] or SAM reductive cleavage induced by use of a substrate analog that cannot undergo turnover.[40] Here we tie both Ω and 5′-dAdo• to RS catalytic turnover, providing evidence for the catalytic competence of both species in a reaction sequence that has been proposed but has not been observed until now and establishing the structure of the 5′-dAdo• engaged in catalysis.

We show that the RS adenosylation of a dehydroalanine-containing peptide substrate catalyzed by PFL-AE proceeds via the Ω organometallic intermediate in which C5′ of a SAM-derived adenosyl moiety is covalently bound to the unique iron of the PFL-AE [4Fe–4S] cluster. The Ω intermediate is observed by EPR spectroscopy after cryogenic trapping at short reaction times (Figure 3) and has an EPR spectrum identical to that of Ω formed upon reaction with the native substrate PFL. Evidence that Ω is a catalytically competent intermediate during adenosylation is provided by the observation of the conversion of Ω to the tertiary C_α radical of the adenosylation product (Ado-Dha-pep•) during cryogenic annealing (Figure 3). This product-radical species was identified by rapid freeze quenching the reaction at longer time points ranging from 8 to 18 s; EPR spectroscopy of these samples showed a clear doublet of doublets signal, consistent with expectations for the tertiary carbon radical that would be formed upon adenosylation of the C_β of the dehydroalanine

residue of Dha-pep (Figure 7). Inspection shows this EPR signal to be the same as that observed upon annealing Ω. Use of SAM and Dha-pep isotopologs provides unequivocal identification of the tertiary C_α radical formed upon addition of 5′-dAdo• to the C_β of Dha (Figure 4).

An adenosylation-product radical has also been characterized for the RS enzyme QueE upon reaction with a substrate analog harboring a double bond at the normal site of H-atom abstraction,[45] suggesting that re-direction of RS H-atom abstraction to adenosylation may be generally achievable by the introduction of double bonds or other reactive groups at the site of RS H-atom abstraction. The RS maturase HydE has been shown to catalyze adenosylation of non-native 1,3-thiazolidine substrates in a reaction that has been structurally dissected.[41] Radical B_{12} enzymes, which show remarkable similarities to RS enzymes,[26] also have a propensity for adenosylation of reactive substrate analogs, as demonstrated by the observation of an adenosylation-product radical formed by methylmalonyl-CoA mutase with the nonnative substrate itaconyl-CoA.[42]

These adenosylation results parallel those observed in the H-atom abstraction reaction of PFL-AE with SAM and PFL, where annealing of Ω produced the product PFL glycyl radical.[19] In both cases, the thermal energy provided by annealing in the frozen state promotes Ω Fe-C bond homolysis to produce a 5′-dAdo• intermediate, which either abstracts the G734 *pro-S* hydrogen atom to generate G734• when PFL is the substrate, or adenosylates the dehydroalanine residue yielding the tertiary Ado-Dha-pep• when Dha-pep is the substrate in the present study. It is interesting to note that an Ω species precedes an organic substrate-based radical upon freeze quenching the reaction of the RS enzyme SuiB at 20 s,[21] suggesting a similar organometallic radical mechanism in this enzyme. Moreover, an Ω species was implicated in the RS enzyme viperin.[22]

An additional EPR signal was observed along with the Ado-Dha-pep• EPR signal over a range of freeze-quench time points from ~8 to ~18 s (Figure 7). It is most prominent at the 8 s freeze-quench time and is most clearly seen by the features outside the high-field and low-field edges of the Ado-Dha-pep• signal, and it can be observed in isolation by subtraction of the Ado-Dha-pep• signal from the experimental spectra (Figure 6). The signal is centered at $g = 2$, and its ^{1}H hyperfine coupling parameters are essentially equivalent to those of photolysis-generated 5′-dAdo•.[37] This result, together with annealing and time course data, in which the radical disappears with a concomitant increase in the product-radical signal, establish that this species indeed is a catalytically competent 5′-dAdo• formed by liberation from Ω and caught in the act of adenosylating the Dha peptide.

This observation of 5′-dAdo• during a catalytic reaction may seem surprising, even remarkable, given that 5′-dAdo• has been thought to be too high in energy to be observed during enzyme turnover.[16] Indeed non-turnover conditions were used to trap the 5′-dAdo• radical in recent reports: cryogenic photolysis in the absence of substrate,[37,39] and radical initiation induced by a non-reactive substrate.[40] In fact, the dearth of direct evidence for the 5′-dAdo• radical has led to a considerable discussion as to whether 5′-dAdo• is a true intermediate species in enzymatic reactions or is instead unobserved during catalysis due to concerted reductive cleavage/H-atom abstraction.[5,36,41] The results reported herein provide

an answer insofar as RS adenosylation reactions are concerned: the 5′-dAdo• radical is a catalytically competent intermediate during RS adenosylation.

To illustrate the adenosylation reaction, a model of the RVS(Dha)YAVR peptide in the active site of PFL-AE was generated from the crystallographically determined structure of PFL-AE, SAM, and RVSGYAV peptide (PDB: 3CB8)[53] by changing the central Gly residue (Gly734 of PFL) to a Dha residue. This model places the olefin of the Dha residue such that radical addition by the 5′-dAdo• would occur on one face of the olefin (Figure 8A). The predicted distance between 5′-C of SAM and C_β of the dehydroalanine (3.7 Å) is comparable to the predicted distance from C5′ to the C_α in the native peptide (3.9 Å), which has the target H-atom of the latter pointing toward and considerably closer to the C5′.[53] Thus, while the adenosylation reaction is thermodynamically more favorable than H-atom abstraction, the reactive 5′-dAdo• must travel further to complete the nucleophilic addition to Dha-pep. Further modeling shows that, once the C–C bond is formed between the peptide and 5′-dAdo•, only a slight change in the active site is required to accommodate the resulting adenosylated product peptide, with the hydrogen bonding interactions between the Tyr35, His37, His202 residues, and the adenosine moiety retained (Figure 8B). The modeling supports the experimental observations that substitution of a dehydroalanine group at the Gly734 position results in facile PFL-AE catalyzed radical SAM adenosylation of the Dha peptide.

CONCLUSIONS

The results presented here demonstrate the sequential formation of three distinct radical intermediates during the PFL-AE catalyzed radical SAM adenosylation reaction: the organometallic intermediate Ω is observed at short freeze-quench times, while intermediate freeze-quench times reveal a mixture of 5′-dAdo• and the product-radical intermediate Ado-Dha-pep•, with only Ado-Dha-pep• observed at the longest freeze-quench times. The loss of 5′-dAdo• with a concomitant gain of Ado-Dha-pep• as the freeze-quench time increases shows that the 5′-dAdo• is a reaction intermediate that converts to Ado-Dha-pep• as the reaction progresses. Thermal annealing of samples containing 5′-dAdo• demonstrates that this species is a catalytically competent intermediate caught in the act of forming the product Ado-Dha-pep•, the first direct observation of 5′-dAdo• as a reaction intermediate.

These results provide the clearest visualization to date of the progression of steps during radical initiation in radical SAM reactions, with Ω undergoing homolytic Fe–C5′ bond cleavage to release 5′-dAdo•, which then reacts with the substrate. They further show that radical SAM adenosylation reactions proceed by the same initiation steps as the more extensively studied H-atom abstraction reactions.

Supplementary Material

Refer to Web version on PubMed Central for supplementary material.

ACKNOWLEDGMENTS

M.A.M. appreciates startup financial support from Montana State University, Bozeman. Computational efforts were performed on the Hyalite High Performance Computing System, operated and supported by University Information Technology Research Cyberinfrastructure at Montana State University.

Funding

This work was supported by the National Institute of General Medical Sciences of the National Institutes of Health (GM131889 to J.B.B., GM111097 to B.M.H., and GM058822 to W.A.V.). M.N.L. (F32GM140713) and R.J.J. (T32GM008382) are supported by the NIH. Funding for Proteomics, Metabolomics, and Mass Spectrometry Facility was provided by the MJ Murdock Charitable Trust and the NIH (P20GM103474). A Bruker UltrafleXtreme MALDI-TOF/TOF mass spectrometer was purchased in part with a grant from the National Center for Research Resources, NIH (S10 RR027109 A).

ABBREVIATIONS

SAM	*S*-adenosyl-L-methionine
RS	radical SAM
5′-dAdo•	5′-deoxyadenosyl radical
PFL-AE	pyruvate formate-lyase activating enzyme
Dha	dehydroalanine
EPR	electron paramagnetic resonance
ENDOR	electron-nuclear double resonance
Dha-pep	dehydroalanine-containing peptide substrate
Ado-Dha-pep•	adenosylated Dha peptide radical
DFT	density functional theory

REFERENCES

(1). Frey PA; Hegeman AD; Ruzicka FJ The radical SAM superfamily. Crit. Rev. Biochem. Mol. Biol 2008, 43, 63–88. [PubMed: 18307109]

(2). Broderick JB; Duffus BR; Duschene KS; Shepard EM Radical S-Adenosylmethionine Enzymes. Chem. Rev 2014, 114, 4229–4317. [PubMed: 24476342]

(3). Landgraf BJ; McCarthy EL; Booker SJ Radical S-adenosylmethionine enzymes in human health and disease. Annu. Rev. Biochem 2016, 85, 485–514. [PubMed: 27145839]

(4). Bridwell-Rabb J; Grell TAJ; Drennan CL A rich man, poor man story of S-adenosylmethionine and cobalamin revisited. Annu. Rev. Biochem 2018, 87, 555–584. [PubMed: 29925255]

(5). Nicolet Y Structure-function relationships of radical of radical SAM enzymes. Nat. Catal 2020, 3, 337–350.

(6). Ding W; Ji X; Zhong Y; Xu K; Zhang Q Adenosylation reactions catalyzed by the radical S-adenosylmethionine superfamily enzymes. Curr. Opin. Chem. Biol 2020, 55, 86–95. [PubMed: 32086168]

(7). Struck A-W; Thompson ML; Wong LS; Micklefield J S-adenosyl-methionine-dependent methyltransferases: highly versatile enzymes in biocatalysis, biosynthesis and other biotechnological applications. ChemBioChem 2012, 13, 2642–2655. [PubMed: 23180741]

(8). Dowling DP; Vey JL; Croft AK; Drennan CL Structural diversity in the AdoMet radical enzyme superfamily. Biochim. Biophys. Acta 2012, 1824, 1178–1195. [PubMed: 22579873]

(9). Krebs C; Broderick WE; Henshaw TF; Broderick JB; Huynh BH Coordination of adenosylmethionine to a unique iron site of the [4Fe-4S] of pyruvate formate-lyase activating enzyme: A Mössbauer spectroscopic study. J. Am. Chem. Soc 2002, 124, 912–913. [PubMed: 11829592]

(10). Walsby CJ; Hong W; Broderick WE; Cheek J; Ortillo D; Broderick JB; Hoffman BM Electron-nuclear double resonance spectroscopic evidence that S-adenosylmethionine binds in contact with the catalytically active $[4Fe\text{-}4S]^{+}$ cluster of pyruvate formate-lyase activating enzyme. J. Am. Chem. Soc 2002, 124, 3143–3151. [PubMed: 11902903]

(11). Walsby CJ; Ortillo D; Broderick WE; Broderick JB; Hoffman BM An anchoring role for FeS Clusters: Chelation of the amino acid moiety of S-adenosylmethionine to the unique iron site of the [4Fe-4S] cluster of pyruvate formate-lyase activating enzyme. J. Am. Chem. Soc 2002, 124, 11270–11271. [PubMed: 12236732]

(12). Walsby CJ; Ortillo D; Yang J; Nnyepi M; Broderick WE; Hoffman BM; Broderick JB Spectroscopic approaches to elucidating novel iron-sulfur chemistry in the ″Radical SAM″ protein superfamily. Inorg. Chem 2005, 44, 727–741. [PubMed: 15859242]

(13). Dey A; Peng Y; Broderick WE; Hedman B; Hodgson KO; Broderick JB; Solomon EI S K-edge XAS and DFT Calculations on SAM Dependent Pyruvate Formate-Lyase Activating Enzyme: Nature of Interaction between the Fe4S4 Cluster and SAM and its Role in Reactivity. J. Am. Chem. Soc 2011, 133, 18656–18662. [PubMed: 21992686]

(14). Henshaw TF; Cheek J; Broderick JB The $[4Fe\text{-}4S]^{+}$ cluster of pyruvate formate-lyase activating enzyme generates the glycyl radical on pyruvate formate-lyase: EPR-detected single turnover. J. Am. Chem. Soc 2000, 122, 8331–8332.

(15). Lieder KW; Booker S; Ruzicka FJ; Beinert H; Reed GH; Frey PA *S*-Adenosylmethionine-dependent reduction of lysine 2,3-aminomutase and observation of the catalytically functional iron-sulfur centers by electron paramagnetic resonance. Biochemistry 1998, 37, 2578–2585. [PubMed: 9485408]

(16). Frey PA; Magnusson OT S-Adenosylmethionine: A wolf in sheep's clothing, or a rich man's adenosylcobalamin? Chem. Rev 2003, 103, 2129–2148. [PubMed: 12797826]

(17). Moss M; Frey PA The role of S-adenosylmethionine in the lysine 2,3-aminomutase reaction. J. Biol. Chem 1987, 262, 14859–14862. [PubMed: 3117791]

(18). Walls WG; Moody JD; McDaniel EC; Villanueva M; Shepard EM; Broderick WE; Broderick JB The B12-independent glycerol dehydratase activating enzyme from Clostridium butyricum cleaves SAM to produce 5′-deoxyadenosine and not 5′-deoxy-5′-(methylthio) adenosine. J. Inorg. Biochem 2021, 227, No. 111662.

(19). Horitani M; Shisler KA; Broderick WE; Hutcheson RU; Duschene KS; Marts AR; Hoffman BM; Broderick JB Radical SAM catalysis via an organometallic intermediate with an Fe-[5′-C]-deoxyadenosyl bond. Science 2016, 352, 822–825. [PubMed: 27174986]

(20). Byer AS; Yang H; McDaniel EC; Kathiresan V; Impano S; Pagnier A; Watts H; Denler C; Vagstad AL; Piel J; Duschene KS; Shepard EM; Shields TP; Scott LG; Lilla EA; Yokoyama K; Broderick WE; Hoffman BM; Broderick JB Paradigm shift for radical S-adenosyl-L-methionine reactions: The organometallic intermediate Ω is central to catalysis. J. Am. Chem. Soc 2018, 140, 8634–8638. [PubMed: 29954180]

(21). Balo AR; Caruso A; Tao L; Tantillo DJ; Seyedsayamdost MR; Britt RD Trapping a cross-linked lysinetryptophan radical in the catalytic cycle of the radical SAM enzyme SuiB. Proc. Natl. Acad. Sci. U. S. A 2021, 118, No. e2101571118.

(22). Ebrahimi KH; Carr SB; McCullagh J; Wickens J; Rees NH; Cantley J; Armstrong FA The radical-SAM enzyme viperin catalyzes reductive addition of a 5′-deoxyadenosyl radical to UDP-glucose in vitro. FEBS Lett 2017, 591, 2394–2405. [PubMed: 28752893]

(23). Ye M; Thompson NB; Brown AC; Suess DLM A synthetic model of enzymatic [Fe4S4]-alkyl intermediates. J. Am. Chem. Soc 2019, 141, 13330–13335. [PubMed: 31373801]

(24). Brown AC; Suess DLM Reversible formation of alkyl radicals at [Fe4S4] clusters and its implications for selectivity in radical SAM enzymes. J. Am. Chem. Soc 2020, 142, 14240–14248. [PubMed: 32696642]

(25). McSkimming A; Sridharan A; Thompson NB; Müller P; Suess DLM An $[Fe4S4]^{3+}$–alkyl cluster stabilized by an expanded scorpionate ligand. J. Am. Chem. Soc 2020, 142, 14314–14323. [PubMed: 32692919]

(26). Broderick WE; Hoffman BM; Broderick JB Mechanism of Radical Initiation in the Radical S-Adenosyl-l-methionine Super-family. Acc. Chem. Res 2018, 51, 2611–2619. [PubMed: 30346729]

(27). Joshi S; Fedoseyenko D; Mahanta N; Manion H; Naseem S; Dairi T; Begley TP Novel enzymology in futalosine-dependent menaquinone biosynthesis. Curr. Opin. Chem. Biol 2018, 47, 134–141. [PubMed: 30447488]

(28). Dairi T An alternative menaquinone biosynthetic pathway operating in microorganisms: an attractive target for drug discovery to pathogenic Helicobacter and Chlamydia strains. J. Antibiot 2009, 62, 347–352.

(29). Joshi S; Mahanta N; Fedoseyenko D; Williams H; Begley TP Aminofutalosine Synthase: Evidence for Captodative and Aryl Radical Intermediates Using beta-Scission and SRN1 Trapping Reactions. J. Am. Chem. Soc 2017, 139, 10952–10955. [PubMed: 28701039]

(30). Zhong Y; Ji X; Zhang Q Radical SAM-Dependent Adenosylation Involved in Bacteriohopanepolyol Biosynthesis. Chin. J. Chem 2020, 38, 39–42.

(31). Sato S; Kudo F; Rohmer M; Eguchi T Characterization of Radical SAM Adenosylhopane Synthase, HpnH, which Catalyzes the 5'-Deoxyadenosyl Radical Addition to Diploptene in the Biosynthesis of C35 Bacteriohopanepolyols. Angew. Chem., Int. Ed 2020, 59, 237–241.

(32). Baraniak J; Moss ML; Frey PA Lysine 2,3-aminomutase. Support for a mechanism of hydrogen transfer involving S-adenosylmethionine. J. Biol. Chem 1989, 264, 1357–1360. [PubMed: 2492274]

(33). Frey PA Travels with carbon-centered radicals. 5′-deoxyadenosine and 5′-deoxyadenosine-5′-yl in radical enzymology. Acc. Chem. Res 2014, 47, 540–549. [PubMed: 24308628]

(34). Magnusson OT; Reed GH; Frey PA Spectroscopic Evidence for the participation of an allylic analogue of the 5′-deoxyadenosyl radical in the reaction of lysine 2,3-aminomutase. J. Am. Chem. Soc 1999, 121, 9764–9765.

(35). Magnusson OT; Reed GH; Frey PA Characterization of an Allylic Analogue of the 5'-Deoxyadenosyl Radical: An Intermediate in the Reaction of Lysine 2,3-Aminomutase. Biochemistry 2001, 40, 7773–7782. [PubMed: 11425303]

(36). Horitani M; Byer AS; Shisler KA; Chandra T; Broderick JB; Hoffman BM Why Nature Uses Radical SAM Enzymes so Widely: Electron Nuclear Double Resonance Studies of Lysine 2,3-Aminomutase Show the 5′-dAdo• ″Free Radical″ is Never Free. J. Am. Chem. Soc 2015, 137, 7111–7121. [PubMed: 25923449]

(37). Yang H; McDaniel EC; Impano S; Byer AS; Jodts RJ; Yokoyama K; Broderick WE; Broderick JB; Hoffman BM The elusive 5′-deoxyadenosyl radical: Captured and Characterized by Electron Paramagnetic Resonance and Electron Nuclear Double Resonance Spectroscopies. J. Am. Chem. Soc 2019, 141, 12139–12146. [PubMed: 31274303]

(38). Yang H; Impano S; Shepard EM; James CD; Broderick WE; Broderick JB; Hoffman BM Photoinduced electron transfer in a radical SAM enzyme generates an S-adenosylmethionine derived methyl radical. J. Am. Chem. Soc 2019, 141, 16117–16124. [PubMed: 31509404]

(39). Impano S; Yang H; Jodts RJ; Pagnier A; Swimley R; McDaniel EC; Shepard EM; Broderick WE; Broderick JB; Hoffman BM Active-Site Controlled, Jahn-Teller Enabled Regioselectivity in Reductive S-C Bond Cleavage of S-Adenosylmethionine (SAM) in Radical-SAM Enzymes. J. Am.Chem. Soc 2021, 143, 335–348. [PubMed: 33372786]

(40). Sayler RI; Stich TA; Joshi S; Cooper N; Shaw JT; Begley TP; Tantillo DJ; Britt RD Trapping and electron paramagnetic resonance characterization of the 5′-dAdo• radical in a radical S-adenosylmethionine enzyme reaction with a non-native substrate. ACS Cent. Sci 2019, 5, 1777–1785. [PubMed: 31807679]

(41). Rohac R; Amara P; Benjdia A; Martin L; Ruffié P; Favier A; Berteau O; Mouesca J-M; Fontecilla-Camps JC; Nicolet Y Carbon-sulfur bond-forming reaction catalysed by the radical SAM enzyme HydE. Nat. Chem 2016, 8, 491–500. [PubMed: 27102684]

(42). Ruetz M; Campanello GC; Purchal M; Shen H; McDevitt L; Gouda H; Wakabayashi S; Zhu J; Rubin EJ; Warncke K; Mootha VK; Koutmos M; Banerjee R Itaconyl-CoA forms a stable biradical in methylmalonyl-CoA mutase and derails its activity and repair. Science 2019, 366, 589–593. [PubMed: 31672889]

(43). Wagner AFV; Demand J; Schilling G; Pils T; Knappe J A dehydroalanyl residue can capture the 5′-dAdo radical generated from SAM by PFL-AE. Biochem. Biophys. Res. Commun 1999, 254, 306–310. [PubMed: 9918833]

(44). Bruender NA; Grell TAJ; Dowling DP; McCarty RM; Drennan CL; Bandarian V 7-Carboxy-7-deazaguanine synthase: A radical S-adenosyl-L-methionine enzyme with polar tendencies. J. Am.Chem. Soc 2017, 139, 1912–1920. [PubMed: 28045519]

(45). Wilcoxen J; Bruender NA; Bandarian V; Britt RD A Radical Intermediate in Bacillus subtilis QueE during Turnover with the Substrate Analogue 6-Carboxypterin. J. Am. Chem. Soc 2018, 140, 1753–1759. [PubMed: 29303575]

(46). Ji X; Li Y; Xie L; Lu H; Ding W; Zhang Q Expanding Radical SAM Chemistry by Using Radical Addition Reactions and SAM Analogues. Angew. Chem., Int. Ed 2016, 55, 11845–11848.

(47). Bhandari DM; Fedoseyenko D; Begley TP Tryptophan Lyase (NosL): A Cornucopia of 5′-Deoxyadenosyl Radical Mediated Transformations. J. Am. Chem. Soc 2016, 138, 16184–16187. [PubMed: 27998091]

(48). Ji X; Mandalapu D; Cheng J; Ding W; Zhang Q Expanding the chemistry of the class C radical SAM methyltransferase NosN by using an allyl analog of SAM. Angew. Chem., Int. Ed 2018, 57, 6601–6604.

(49). Wu Y; Wu R; Mandalapu D; Ji X; Chen T; Ding W; Zhang Q Radical SAM-dependent adenosylation catalyzed by l-tyrosine lyases. Org. Biomol. Chem 2019, 17, 1809–1812. [PubMed: 30520933]

(50). Knappe J; Neugebauer FA; Blaschkowski HP; Gänzler M Post-translational activation introduces a free radical into pyruvate formate-lyase. Proc. Natl. Acad. Sci. U. S. A 1984, 81, 1332–1335. [PubMed: 6369325]

(51). Wagner AFV; Frey M; Neugebauer FA; Schäfer W; Knappe J The free radical in pyruvate formate-lyase is located on glycine-734. Proc. Natl. Acad. Sci. U. S. A 1992, 89, 996–1000. [PubMed: 1310545]

(52). Frey M; Rothe M; Wagner AFV; Knappe J Adenosylmethionine-dependent synthesis of the glycyl radical in pyruvate formate-lyase by abstraction of the glycine C-2 pro-S hydrogen atom. J. Biol. Chem 1994, 269, 12432–12437. [PubMed: 8175649]

(53). Vey JL; Yang J; Li M; Broderick WE; Broderick JB; Drennan CL Structural basis for glycyl radical formation by pyruvate formate-lyase activating enzyme. Proc. Natl. Acad. Sci. U. S. A 2008, 105, 16137–16141. [PubMed: 18852451]

(54). Morrison PM; Foley PJ; Warriner SL; Webb ME Chemical generation and modification of peptides containing multiple dehydroalanines. Chem. Commun 2015, 51, 13470–13473.

(55). Chalker JM; Lercher L; Rose NR; Schofield CJ; Davis BG Conversion of cysteine into dehydroalanine enables access to synthetic histones bearing diverse post-translational modifications. Angew. Chem., Int. Ed 2012, 51, 1835–1839.

(56). Byer AS; McDaniel EC; Impano S; Broderick WE; Broderick JB Mechanistic Studies of Radical SAM Enzymes: Pyruvate Formate-Lyase Activating Enzyme and Lysine 2,3-Amino-mutase Case Studies. Methods Enzymol 2018, 606, 269–318. [PubMed: 30097096]

(57). Stoll S; Schweiger A EasySpin, a comprehensive software package for spectral simulation and analysis in EPR. J. Magn. Res 2006, 178, 42–55.

(58). Schrodinger L The PyMOL Molecular Graphics System, Version 2.3.4, 2019.

(59). Neese F The ORCA program system. Comput. Mol. Sci 2012, 2, 73–78.

(60). Valeev EF Libint: A library for the evaluation of molecular integrals of many-body operators over Gaussian functions Version 2.6.0, 2019. http://libint.valeyev.net/.

(61). Lehtola S; Steigemann C; Oliveira MJT; Marques MAL Recent developments in libxc — A comprehensive library of functionals for density functional theory. SoftwareX 2018, 7, 1–5.

(62). Avogadro: an open-source molecular builder and visualization tool, Version 1.2.0, 2017.

(63). Hanwell MD; Curtis DE; Lonie DC; Vandermeersch T; Zurek E; Hutchison GR Avogadro: an advanced semantic chemical editor, visualization, and analysis platform. J. Cheminform 2012, 4, 17. [PubMed: 22889332]

(64). Becke AD Density-functional exchange-energy approximation with correct asymptotic behavior. Phys. Rev. A: At., Mol., Opt. Phys 1988, 38, 3098–3100.

(65). Lee C; Yang W; Parr RG Development of the Colle-Salvetti correlation energy formula into a functional of the electron density. Phys. Rev. B: Condens. Matter Mater. Phys 1988, 37, 785–789.

(66). Perdew JP Density-functional approximation for the correlation-energy of the inhomogeneous electron-gas. Phys. Rev. B: Condens. Matter Mater. Phys 1986, 33, 8822–8824.

(67). Weigend F; Ahlrichs R Balanced basis sets of split valence, triple zeta valence and quadruple zeta valence quality for H to Rn: Design and assessment of accuracy. J. Chem. Phys 2005, 7, 3297–3305.

(68). Weigend F Accurate Coulomb-fitting basis sets for H to Rn. Phys. Chem. Chem. Phys 2006, 8, 1057–1065. [PubMed: 16633586]

(69). Barone V In Recent Advances in Density Functional Methods; World Scientific: Singapore, 1995; p 287.

(70). Barone V; Cossi M; Tomasi J A new definition of cavities for the computation of solvation free energies by the polarizable continuum model. J. Chem. Phys 1997, 107, 3210–3221.

(71). Neese F Efficient and accurate approximations to the molecular spin-orbit coupling operator and their use in molecular gtensor calculations. J. Chem. Phys 2005, 122, 034107.

(72). Pagnier A; Yang H; Jodts RJ; James CD; Shepard EM; Impano S; Broderick WE; Hoffman BM; Broderick JB Radical SAM enzyme spore photoproduct lyase: Properties of the W organometallic interrmediate and identification of stable protein radicals formed during substrate-free turnover. J. Am. Chem. Soc 2020, 142, 18652–18660. [PubMed: 32966073]

(73). Impano S; Yang H; Shepard EM; Swimley R; Pagnier A; Broderick WE; Hoffman BM; Broderick JB S-Adenosyl-L-ethionine is a catalytically competent analog of S-adenosyl-l-methionine (SAM) in the radical SAM enzyme HydG. Angew. Chem., Int. Ed 2021, 60, 4666–4672.

(74). Nnyepi MR; Peng Y; Broderick JB Inactivation of E. coli pyruvate formate-lyase: Role of AdhE and small molecules. Arch. Biochem. Biophys 2007, 459, 1–9. [PubMed: 17280641]

(75). Becker A; Fritz-Wolf K; Kabsch W; Knappe J; Schultz S; Wagner AFV Structure and mechanism of the glycyl radical enzyme pyruvate formate-lyase. Nat. Struct. Biol 1999, 6, 969–975. [PubMed: 10504733]

(76). Peng Y; Veneziano SE; Gillispie GD; Broderick JB Pyruvate formate-lyase, Evidence for an open conformation favored in the presence of its activating enzyme. J. Biol. Chem 2010, 285, 27224–27231. [PubMed: 20571026]

(77). Donnan PH; Mansoorabadi SO Broken-Symmetry Density Functional Theory Analysis of the W Intermediate in Radical SAdenosyl-L-methionine Enzymes: Evidence for a Near-Attach Conformer over an Organometallic Species. J. Am. Chem. Soc 2022, DOI: 10.1021/jacs.2c00678.

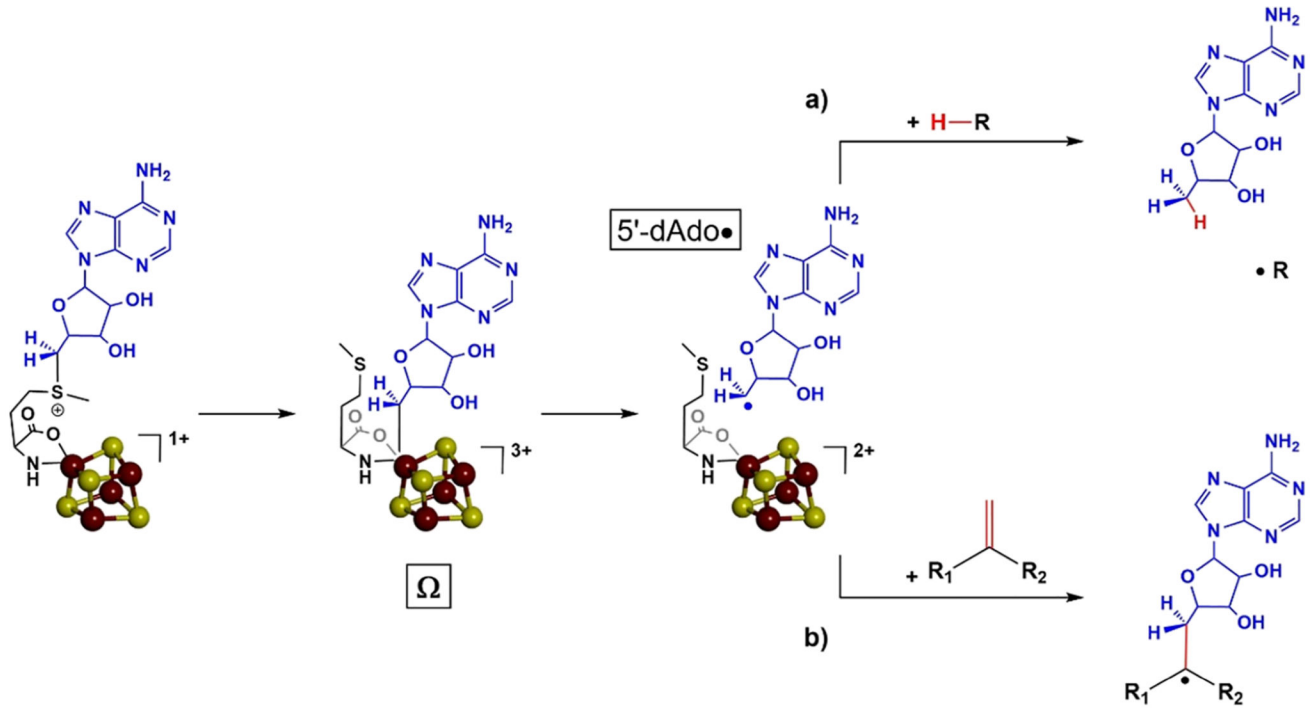

Figure 1.

5′-Deoxyadenosyl radical (5′-dAdo•) generated from reductive cleavage by RS enzyme and subsequent reactivity. Pathway (a) hydrogen atom abstraction from the substrate resulting in substrate radical. Pathway (b) adenosylation of a substrate via 5′-dAdo• addition to sp^2 carbon.

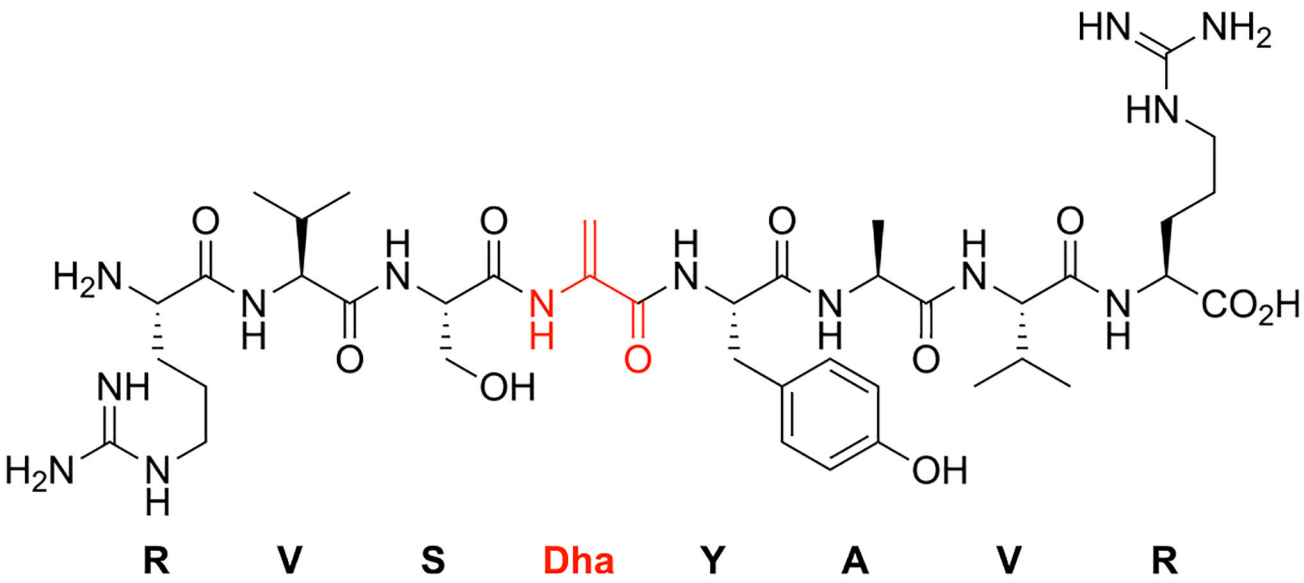

Figure 2.
Structure of the 8-mer Dha-pep.

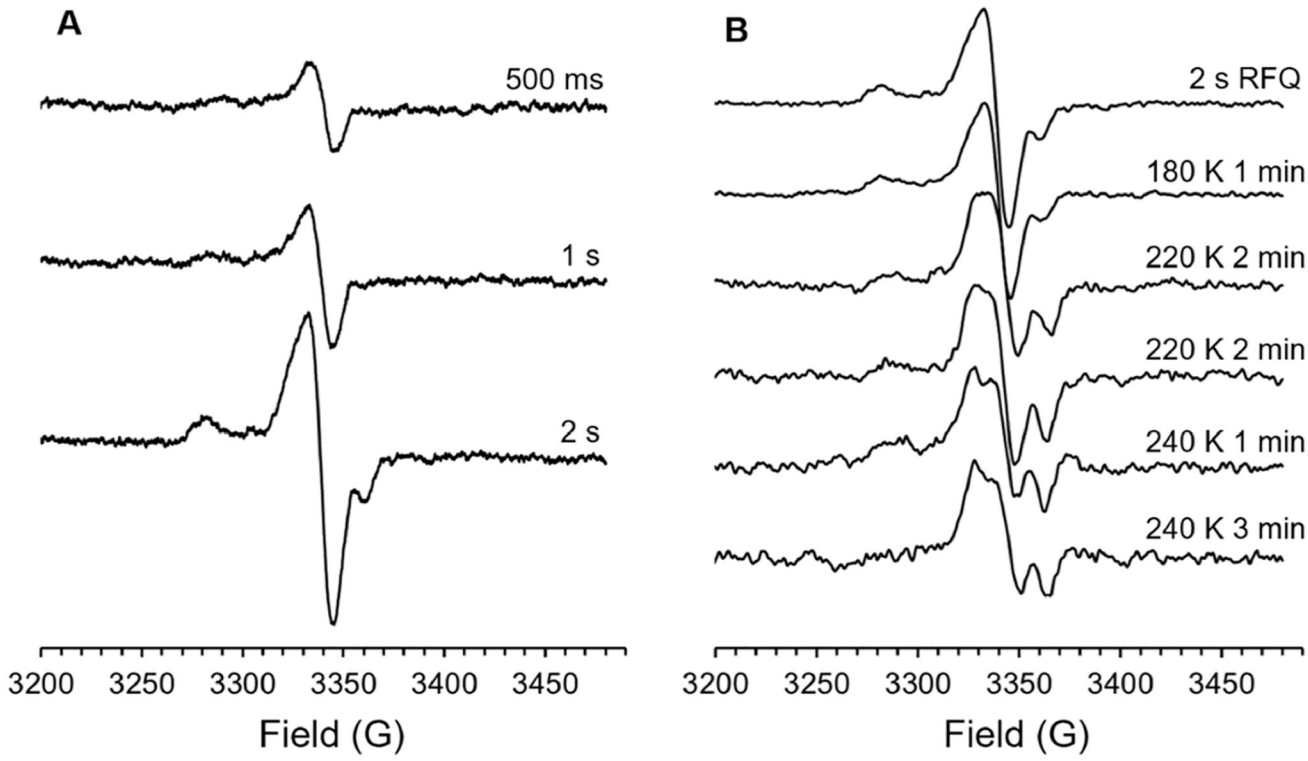

Figure 3.

RFQ and annealing of the PFL-AE/SAM/Dha-pep reaction. (A) RFQ of the reaction of PFL-AE with SAM and Dha-pep at 500 ms, 1, and 2 s shows the increasing intensity of an EPR signal characteristic of the organometallic intermediate Ω. (B) Cryogenic annealing of the 2 s RFQ sample at the temperatures and times shown results in conversion of Ω to a new radical species. The signal from this species is saturation broadened at the observation temperature of 40 K, chosen because Ω is not observable at the higher temperatures optimal for the radical. EPR conditions: microwave frequency, 9.375 GHz; modulation amplitude, 5 G, T = 40 K.

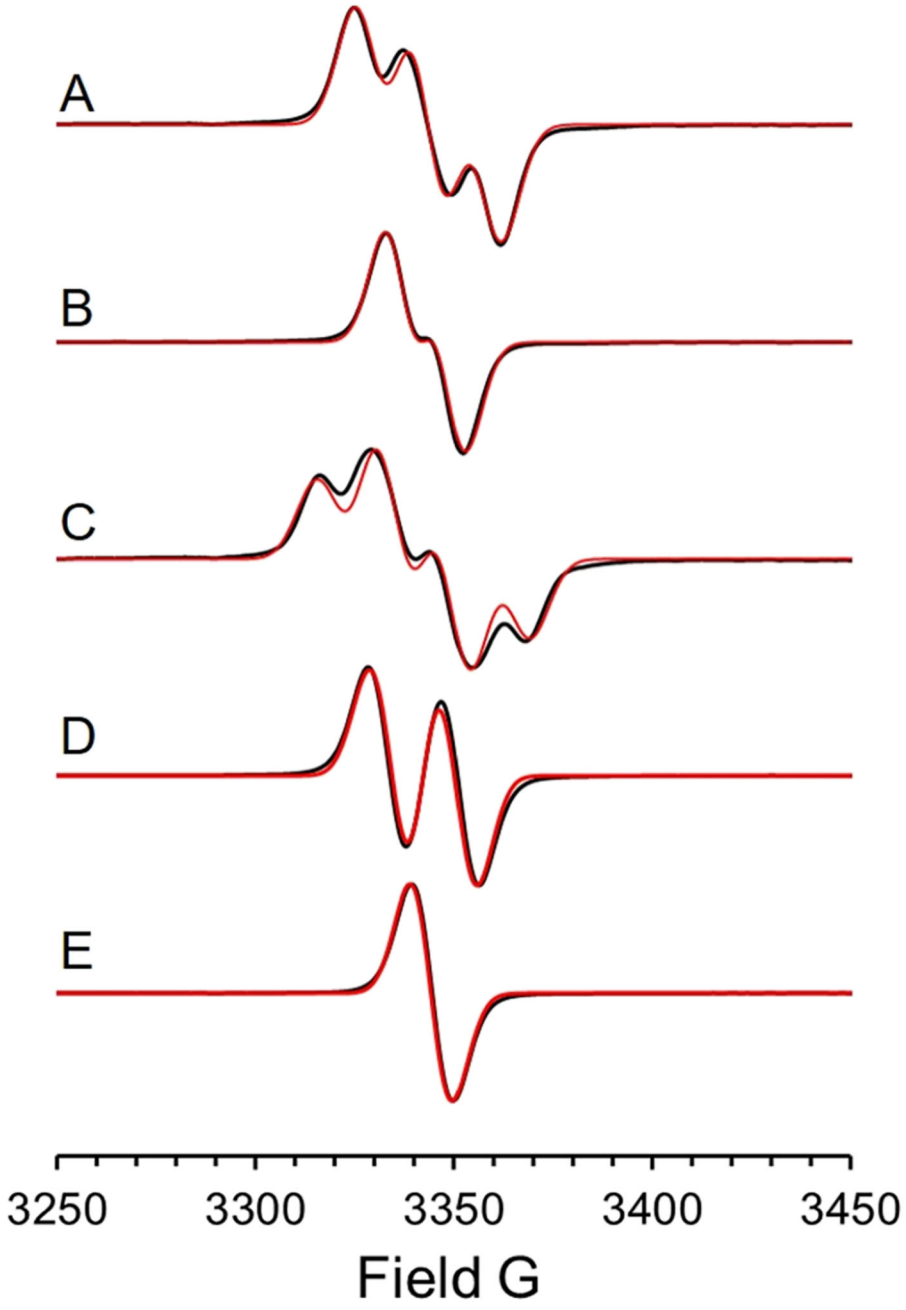

Figure 4.

Normalized 70 K X-band EPR spectra (black) and simulations (red) of the Ado-Dha-pep• generated from the reaction of reduced PFL-AE, SAM, and Dha-pep at RT then freeze-quenched at ~8 s. (A) Reaction using natural abundance (N.A.) SAM and Dha-pep. (B) Reaction was carried out using D_2-Dha-pep. (C) Reaction using [adenosyl-$^{13}C_{10}$,$^{15}N_5$]-SAM. (D) Reaction using natural abundance SAM and Dha-pep was carried out in 95% D_2O. (E) Reaction using natural abundance SAM and D_2-Dha-pep was carried out in 95% D_2O. Total spin quantitations in (A–E) range from 11 to 20 μM. EPR conditions: microwave frequency, 9.38 GHz; modulation, 3 G, T = 70 K. Simulations were generated

with Easyspin[54] with g-tensor = [2.0047 2.0039 2.0025] and hyperfine tensors $a_{iso}(H_a)$ = 45 MHz, a_{iso}(N–H) = 30 MHz, and $a_{iso}(^{13}C(5'))$ = 48 MHz.

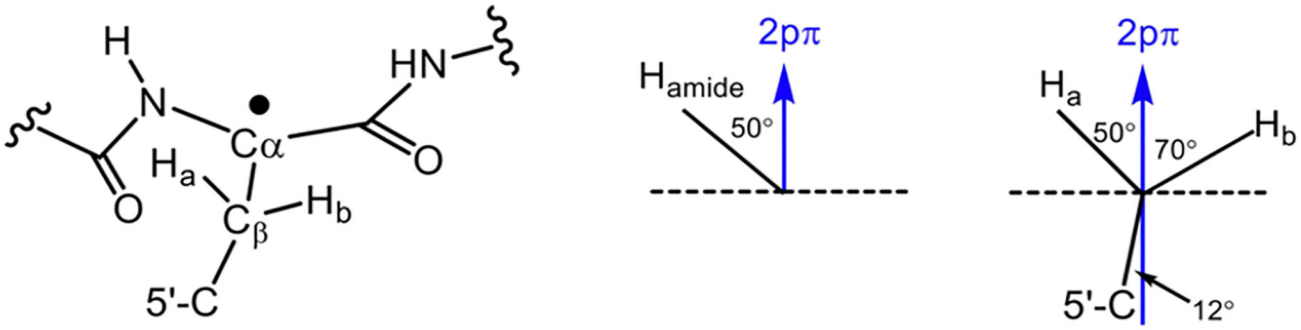

Figure 5.

Structure considered for the Ado-Dha-pep•. Left, depiction of the fixed geometry of the Ado-Dha-pep•. Center, illustration of the dihedral angle between the 2pπ orbital on C_α and the amide N–H bond for the fixed geometry observed in the PFL-AE crystal structure, as viewed down the C_α–N_{amide} bond. Right, illustration of the dihedral angles between the 2pπ orbital on C_α and the C_β–H and C_β–C5′ bonds, viewed down the C_α–C_β bond. The plane of the sp^2 C_α, N_{amide}, and C_β is represented by a dashed line.

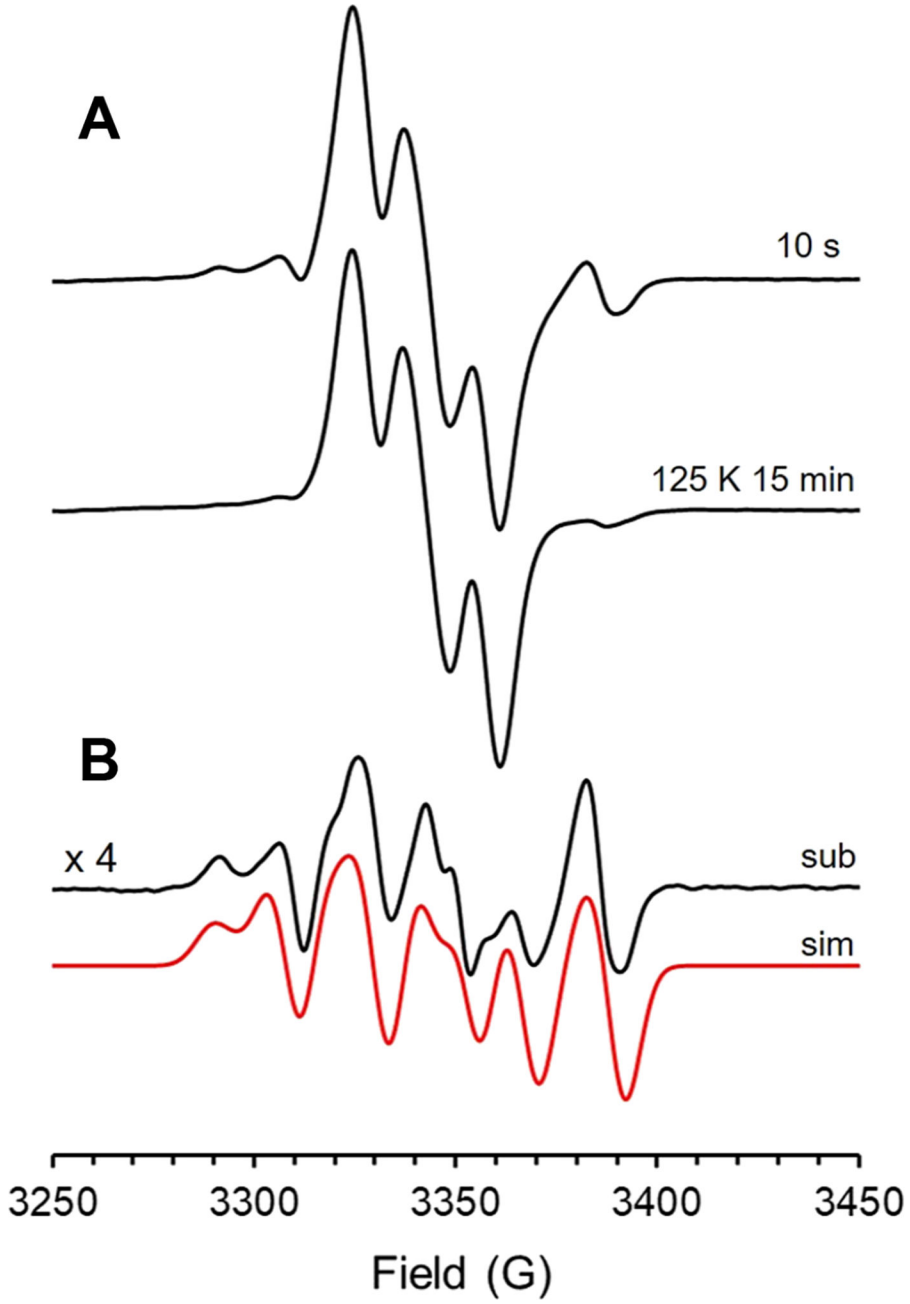

Figure 6.

EPR spectra at 40 K of a 10 s freeze-quench sample before and after annealing reveal the presence of 5′-dAdo•. (A) The CW X-band EPR spectra were recorded at 40 K of the 10 s freeze-quench reaction of PFL-AE, SAM, and Dha-pep before and after annealing at 125 K for 15 min. (B) The difference spectrum generated by subtracting the post-anneal spectrum from the pre-anneal spectrum is shown in black, with the simulation in red. For spin quantitation, see Table S2. EPR conditions: microwave frequency, 9.38 GHz; modulation amplitude, 3 G, T = 40 K.

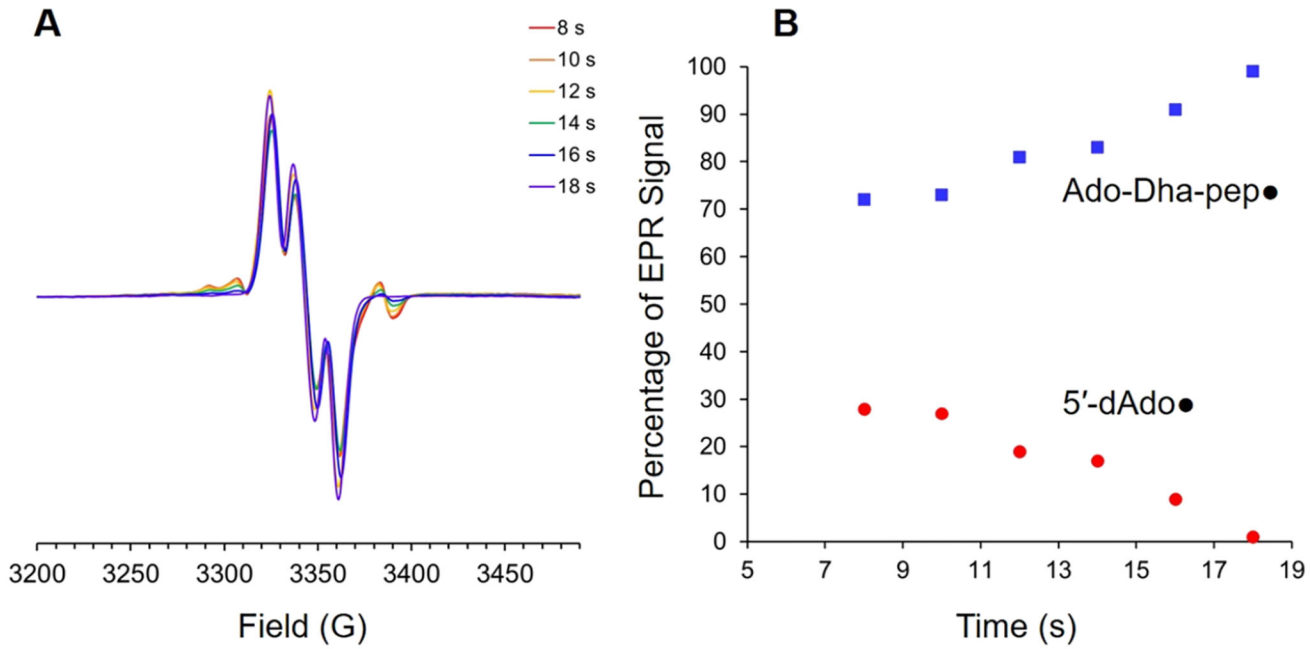

Figure 7.

EPR spectra of freeze-quench time course samples from 8 to 18 s. (A) The CW X-band EPR spectra recorded at 40 K of reactions of PFL-AE, SAM, and Dha-pep freeze-quenched at times from 8 to 18 s. (B) Spectra in panel A were simulated to estimate contributions from the 5′-dAdo• and the Ado-Dha-pep• at each time point. For spin quantitation, see Table S4. EPR conditions: microwave frequency, 9.38 GHz; modulation amplitude, 3 G, T = 40 K.

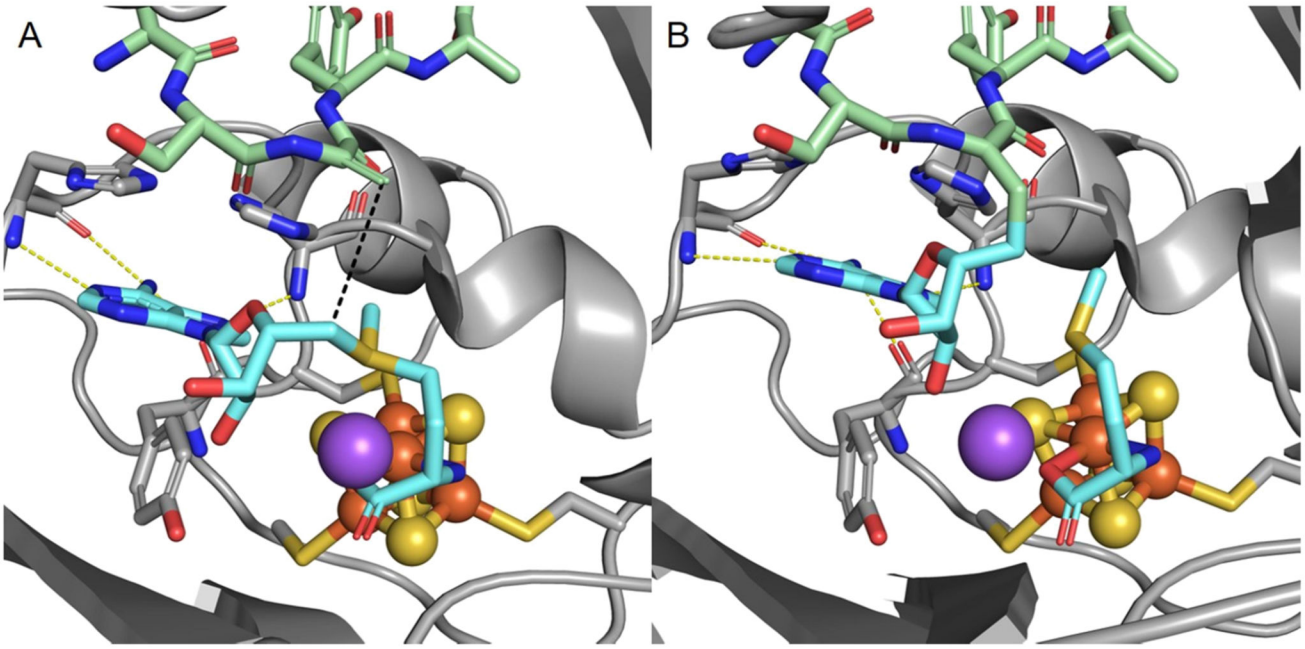

Figure 8.

Models of the Dha peptide and its adenosylated product in the PFL-AE active site from PDB 3CB8. The 4Fe–4S cluster (orange and yellow), sodium ion (purple), SAM (cyan carbons), and peptide (green carbons) are depicted in sticks with oxygen atoms colored red and nitrogen atoms colored blue. Hydrogen bonding interactions of PFL-AE to the adenosine of SAM are yellow dashed lines. (A) Representation of the Dha-pep in the active site of PFL-AE where the black dashed line indicates the 3.7 Å distance from 5′-C to C_{β}. (B) Representation of the Ado-Dha-pep• in the active site of PFL-AE showing the H-bonding from the protein active site to the adenosine is retained.

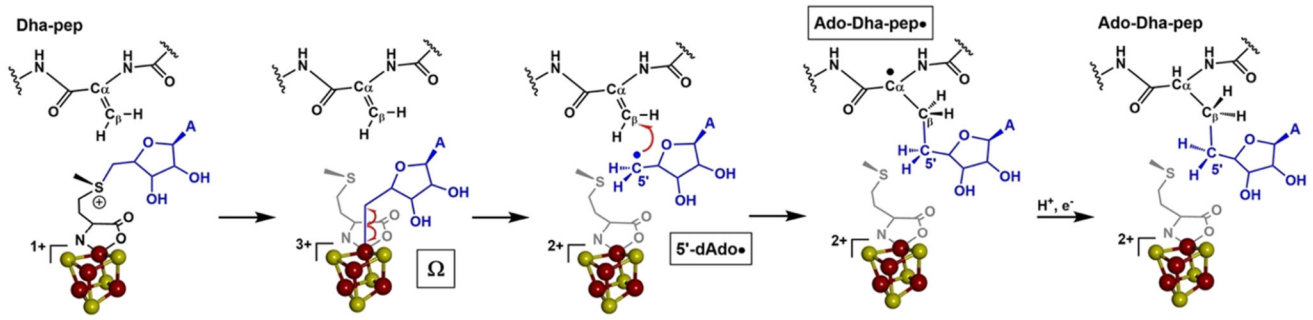

Scheme 1.
Capture of a Tertiary Carbon Radical Intermediate

Table 1.

Hyperfine Tensors (in MHz) from Experimental Simulations and DFT Calculations Using a Truncated Ado-Dha-pep• Model

	exptl sims	calc fixed geometry	calc planar conformation
C_{β}–H_a	45	50	32
C_{β}–H_b	10	10	15
N–H	30	35	8
5′-^{13}C	48	57	53